

### 2.3 Magnetic structures of the elements

As we have seen, the ‘exotic spin configurations’ first observed by Koehler and his colleagues in the heavy rare earths may be understood as the result of a compromise between the competing magnetic interactions to which the moments are subjected. The complex changes which occur as the temperature is varied stem primarily from the temperature dependence of the expectation values of the terms in the MF Hamiltonian (2.1.16). The *crystal-field parameters*  $B_i^m$  are expected to change little with temperature but, as shown in the previous section, the variation of the expectation values  $\langle O_i^m \rangle$  of the *Stevens operators* may give rise to a very pronounced temperature dependence of the anisotropy forces, including the magnetoelastic effects. The contribution from the *two-ion coupling* generally varies more slowly, since the exchange field is proportional to  $\langle \mathbf{J}_j \rangle$  or  $\sigma$ , but changes in the magnitude and orientation of the ordered moments alter the band structure of the conduction electrons, which in turn modifies the *indirect exchange*  $\mathcal{J}(ij)$ . Hence the Fourier transform  $\mathcal{J}(\mathbf{q})$ , and in particular the value  $\mathbf{Q}$  at which it attains its maximum, may change with temperature in the ordered phase. In addition, the possibility that *anisotropic two-ion coupling* may be of importance implies that the effective parameters of the simple MF Hamiltonian (2.1.16) may all depend on the magnitude and orientation of the moments.

The anisotropy forces favour a set of crystallographic directions, related by a rotational symmetry operator, along which the moments tend to align themselves. In particular, the low-order crystal-field term  $B_2^0 \langle O_2^0(\mathbf{J}) \rangle$  gives rise to an *axial anisotropy*, which strives to confine the magnetization either to the basal plane or along the  $c$ -axis, and declines relatively slowly with temperature. Except for Gd, the rare earth elements all have a  $\mathcal{J}(\mathbf{q})$  with a maximum at  $\mathbf{Q} \neq \mathbf{0}$ , reflecting the complexities of the Fermi surface and corresponding to a periodicity which is not generally commensurable with the lattice. Transverse and longitudinal magnetic structures can accommodate both the anisotropy and the periodicity constraints at high temperatures, with respectively uniform helical or longitudinal-wave configurations of the moments, characterized by a single wave-vector. As the temperature is lowered, however,

conditions develop which favour commensurable structures, including the ferromagnet. The *hexagonal anisotropy* distorts the helical structure, while the development of higher harmonics, assisted by the axial-anisotropy forces, favours commensurability in the longitudinal structure. The *higher-order axial-anisotropy terms* may also tend to pull the moments away from their planar or axial orientations. The application of a *magnetic field* requires further compromises, until it is so great that it coerces all the moments into alignment.

The variation of temperature and field thus reveals a rich variety of intermediate phase transitions to different structures. Most of these transitions are discontinuous, but occasionally a second-order transition is observed. In the following, we will discuss the relation between the *interactions*, and their variation, and the *magnetic structures* in the rare earths. We shall give a summary of the rather complete understanding which has been attained of the heavy elements, followed by a brief discussion of the complex structures of Nd, which is the only light rare earth which has been studied in comparable detail. The effect of a magnetic field will be exemplified by a description of the magnetization of Ho. Finally we will consider the new features which emerge when one dimension of the magnetic lattice is bounded, illustrated by some of the results from the rapidly developing study of thin films and superlattices.

### 2.3.1 Bulk magnetic structures

The manner in which the competing interactions express themselves is very well illustrated by the heavy hcp rare earths. In their magnetically ordered phases, all the moments in a particular plane normal to the  $c$ -axis are aligned, but their relative orientations may change from plane to plane. Fig. 1.19 illustrates some of the simpler of these structures, while the transition temperatures  $T_N$  and  $T_C$  to ordered states, respectively without and with a net moment, are given in Table 1.6.

Gd is magnetically by far the simplest of the rare earths. The exchange favours ferromagnetism and the  $4f$  charge-cloud is spherically symmetric, so that the crystal-field interactions (1.4.4) are zero. However there is a residual magnetic anisotropy, which causes the moments to point preferentially along the  $c$ -axis just below  $T_C$ . At lower temperatures, the easy axis begins to deviate towards the basal plane, reaching a maximum tilt angle of  $60^\circ$  at 180 K before decreasing to just below  $30^\circ$  at 4.2 K (Corner and Tanner 1976). The anisotropy parameters are typically two or three orders of magnitude smaller than those of the other heavy rare earths (Mishima *et al.* 1976). Since the  $c/a$  ratio of Table 1.2 is less than the ideal value, the dipolar coupling induces an anisotropy, discussed in Section 5.5.1, which tends to hold the moments along the  $c$ -direction and has roughly the observed magnitude (Brooks and Good-

ings 1968). There is in addition a competing anisotropy, which has its origin in the spin-orbit coupling (1.2.13) of the conduction electron gas, which restricts the free rotation of the spins relative to the lattice. The indirect-exchange interaction then ensures that the localized spins are correspondingly constrained. The magnitude of this effect could in principle be calculated from the electronic structure, at least at absolute zero, but no serious attempts have yet been made to do so.

The small anisotropy of Gd leads to an unusual sequence of structures when it is diluted with Y. The latter has a very strong tendency to impose a periodic magnetic structure on dissolved rare earth moments (Rainford *et al.* 1988a; Caudron *et al.* 1990) and, in a concentration above about 30% in Gd, induces a helical structure below  $T_N$ . The magnetic behaviour of these alloys is completely dominated by the exchange, and the transition to the ferromagnetic structure, both with increasing Gd concentration and, as occurs if the Y concentration is not too high, with decreasing temperature, takes place by a continuous reduction of the turn angle of the helix (Palmer *et al.* 1986), as the peak in  $\mathcal{J}(\mathbf{q})$  moves smoothly to the origin. At higher Y concentrations, a longitudinal wave is also formed along the  $c$ -axis, over a temperature range and with a wave-vector which are different from those of the helix. As discussed in Section 2.1.5, this behaviour shows explicitly that the exchange must be anisotropic. Furthermore, at Y concentrations just above the critical value for the formation of a helix, a ferromagnetic structure, with the easy direction along the  $c$ -axis, forms at  $T_C$ , is transformed into a basal-plane helix through a first-order transition at a lower temperature  $T_N$ , and at an even lower temperature transforms back into the aforementioned ferromagnetic structure, with the moments canted away from the  $c$ -direction.

Tb and Dy both have large axial anisotropies which confine the moments to their basal planes, and the peaks in  $\mathcal{J}(\mathbf{q})$ , illustrated in Fig. 1.17, induce helical structures at the respective Néel temperatures. In Tb, this peak is very small, and the spin-wave measurements illustrated in Fig. 6.1 indicate that it becomes even smaller as the helical phase is established and the superzone energy-gaps grow. Simultaneously, the (negative) anisotropy energy in the ferromagnetic phase increases, particularly the cylindrically-symmetric magnetoelastic term proportional to  $C^2$  in (2.2.27), which makes no contribution in the helical phase because of lattice clamping. Consequently, this anisotropy energy overwhelms the exchange-energy difference (1.5.35) only ten degrees below  $T_N$ , and a first-order transition occurs to a ferromagnetic structure. The peak in the exchange function in Dy is more robust, and the helical phase correspondingly more stable but, as we have discussed in Section 1.5, a ferromagnetic transition ultimately takes place at 85 K.

An instructive example of competing anisotropy forces has been observed in a  $\text{Tb}_{0.5}\text{Dy}_{0.5}$  crystal (Spano *et al.* 1988). This alloy, as would be anticipated, forms a helical structure at 206 K, and transforms into a ferromagnet at 152 K. At this temperature, the predominant anisotropy is due to the Tb magnetoelastic forces in (2.2.28), since the coefficient  $A$  is almost zero for Dy (Martin and Rhyne 1977), and the hexagonal crystal-field anisotropy for both types of ion has renormalized to a very small value. Consequently, the easy axis of magnetization is the  $b$ -axis, as in pure Tb. As the temperature is further reduced, however, the crystal-field contribution grows, roughly as  $\sigma^{21}$ , and since it is much greater for Dy than Tb, the easy axis switches at about 100 K to the  $a$ -direction, as in pure Dy.

**Table 2.1.** Crystal-field parameters (meV).

	$B_2^0$	$B_4^0$	$B_6^0$	$B_6^6$
Ho	0.024	0.0	$-9.6 \cdot 10^{-7}$	$9.2 \cdot 10^{-6}$
Er	-0.027	$-0.3 \cdot 10^{-4}$	$1.3 \cdot 10^{-6}$	$-9.0 \cdot 10^{-6}$
Tm	-0.096	0.0	$-9.2 \cdot 10^{-6}$	$8.9 \cdot 10^{-5}$

Compared with these relatively straightforward systems, the behaviour of the remainder of the magnetic heavy rare earth series, Ho, Er, and Tm, is more intriguing. As illustrated in Fig. 1.17, the peaks in  $\mathcal{J}(\mathbf{q})$  are large, so that periodic structures are stabilized down to low temperatures. The crystal-field anisotropy also allows the moments to move out of the plane. In Table 2.1 are given the anisotropy parameters deduced from studies of the magnetic structures and excitations. Although these must to some extent be considered as effective values, subtracting for example the effects of two-ion and magnetoelastic anisotropy, they are among the best estimates which we have for the crystal fields in the rare earths, and they correlate well with the Stevens factors of Table 1.4.

Ho demonstrates the interplay of the various interactions in an exemplary manner. The positive value of  $B_2^0$  and the peak in the exchange function again stabilize the helix at  $T_N$ . The peak value  $\mathcal{J}(\mathbf{Q})$  is now so large, however, that the cylindrically-symmetric magnetoelastic energy, which is substantially smaller than that of Dy, is unable to induce a ferromagnetic transition. On the other hand, the hexagonal crystal-field anisotropy is nearly three times as big as in Dy, and distorts the helix drastically when the temperature is reduced, as revealed by the appear-

ance of higher harmonics in neutron diffraction (Koehler *et al.* 1966). As illustrated in Fig. 2.4, the peak in  $\mathcal{J}(\mathbf{q})$  simultaneously moves to smaller values of  $\mathbf{q}$ , and the  $\mathbf{Q}$  of the magnetic structure decreases correspondingly. However this change does not occur uniformly with temperature, but rather a series of *commensurable* wave-vectors is traversed, with apparently discontinuous jumps between them (Gibbs *et al.* 1985). At 20 K, a second-order transition to a shallow cone structure, with an opening angle which decreases continuously towards  $80^\circ$  as the temperature is lowered, is observed. The helical component is commensurable with the lattice, with an average turn angle of  $30^\circ$ , but the moments are strongly bunched around the easy  $b$ -axes, as shown in Fig. 1.20.

To interpret this rich variety of phenomena, we will use the model of Larsen *et al.* (1987). The Hamiltonian which they constructed has

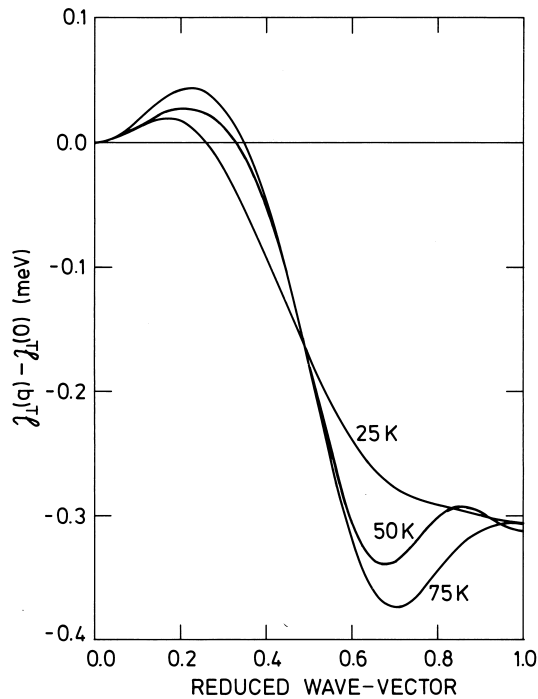


**Fig. 2.4.** The Fourier transform, for wave-vectors in the  $c$ -direction, of the indirect-exchange interaction in Ho at different temperatures, deduced from the magnetic excitations and used in the calculation of the structures. The maximum in  $\mathcal{J}_\perp(\mathbf{q})$  increases in magnitude and moves to larger wave-vectors as the temperature is increased, leading to a decrease in the repeat distance of the periodic structures.

the form of (2.1.1), augmented by the magnetic dipole–dipole interaction (1.4.26) which, as we shall see, is of crucial importance. The crystal-field parameters  $B_l^m$  were determined primarily from a fit to the magnetic structures and magnetization curves at low temperatures, shown in Fig. 1.20, and the temperature dependence of these parameters was assumed to be negligible. The initial values for the isotropic Heisenberg exchange were taken from an analysis of the spin waves in Ho (Jensen 1988a), and depend explicitly on the temperature, as shown in Fig. 2.4. They were adjusted slightly (Mackintosh and Jensen 1990) to reproduce correctly the transition fields from the helical phase, but remain consistent with the spin-wave data, within the experimental error. The magnetic properties are calculated by means of the method described in Section 2.1.2, assuming an initial distribution  $\langle \mathbf{J}_i \rangle$  of the moments at a given temperature. The structure is taken to be commensurate, with a repeat distance, deduced from experimental data, which may be as high as 50–100 atomic layers for the more complex configurations. The assumed values of  $\langle \mathbf{J}_i \rangle$  are inserted into the Hamiltonian and a new set of moments calculated, using the mean-field method to reduce the two-ion term to the single-ion form. This procedure is repeated until self-consistency is attained. The free energy and the moments on the different sites can then readily be calculated for the self-consistent structure.

The results of such self-consistent calculations for different temperatures and commensurate periodicities are shown in Fig. 2.5. The data indicate that  $B_4^0$  is zero, to within the experimental error, whereas  $B_6^0$  has the opposite sign to  $B_2^0$ . As the temperature is reduced in the helical phase and  $B_6^0 \langle O_6^0 \rangle$  increases, this term tends to pull the moments out of the plane. If the only two-ion coupling were the isotropic exchange, this would give rise to a continuous transition to a tilted helix, which reduces the exchange energy more effectively than the cone (Elliott 1971, Sherrington 1972). However, the dipolar interaction strongly favours a ferromagnetic orientation of the  $c$ -axis moments, because the dipolar energy associated with a longitudinal wave is very high, as we discuss in detail in Section 5.5.1. Consequently, the dipolar contribution shifts the position of the maximum in  $\mathcal{J}_{\parallel}(\mathbf{q})$  from  $\mathbf{q} = \mathbf{Q}$  to zero wave-vector, as illustrated in Fig. 5.7, and the vanishing of the axial anisotropy (2.2.33) at  $\mathbf{q} = \mathbf{0}$  leads to a second-order transition at  $T'_N$  to the cone phase. In this special case, we can therefore conclude that it is the temperature dependence of  $B_6^0 \langle O_6^0 \rangle$  which drives the helix into instability, and that the dipolar interaction chooses the cone, rather than the tilted helix, as the stable low-temperature phase.

At 4 K, in the cone phase, the large hexagonal anisotropy causes the helical component of the moments to bunch around the easy directions of magnetization, in the twelve-layer structure described by eqn (1.5.3),

so that the constant angle  $\phi$  in the plane between any moment and the nearest  $b$ -axis is only  $5.8^\circ$ , as shown in Fig. 2.5(a), compared with the  $15^\circ$  which corresponds to a uniform helix. As the temperature is increased, the expectation value  $\langle O_6^6 \rangle$  decreases with the relative magnetization, roughly like  $\sigma^{21}$ , and  $\phi$  increases correspondingly. Simultaneously  $\mathbf{Q}$  tends to increase, reflecting the change in the position of the maximum

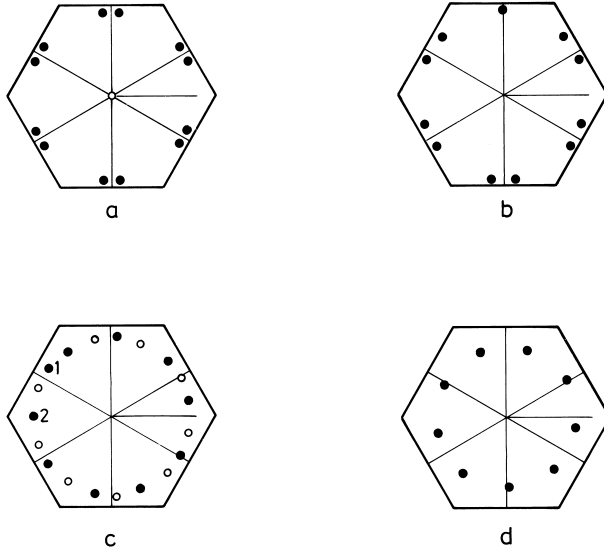


**Fig. 2.5.** The self-consistent periodic structures in Ho, calculated at different temperatures. Each circle represents the magnitude and direction of the ordered moment in a specific plane, relative to the size of the moment at absolute zero ( $10 \mu_B$ ), indicated by the length of the horizontal lines. The orientation of moments in adjacent planes is depicted by the positions of neighbouring circles.

- (a) The 12-layer zero-spin-slip structure at 4 K. The open circle in the centre indicates the ferromagnetic component in the cone structure.
- (b) The 11-layer one-spin-slip structure at 25 K. The bunched pairs of moments are disposed unsymmetrically with respect to the easy axis in the vicinity of the spin slip.
- (c) The 19-layer structure at 50 K. The orientation of the moments in successive layers is determined by following first the filled circles in an anticlockwise direction, as indicated, and then the open circles.
- (d) The 9-layer trigonal structure at 75 K. This may be looked upon as a three-spin-slip structure, but the bunching is so slight that it is more useful to regard it as an almost regular helix, in which every third plane aligns its moments close to an easy axis, in order to reduce the anisotropy energy.

in  $\mathcal{J}(\mathbf{q})$ , so that the structure at 25 K has reduced its periodicity to 11 layers by introducing a regularly-spaced series of *spin slips*, at which one plane of a bunched doublet is omitted while the remaining member orients its moments along the adjacent easy axis. The configuration of Fig. 2.5(b), in which one spin slip is introduced for each repeat distance of the perfect commensurate structure, is the primordial spin-slip structure and has a number of interesting features. It is particularly stable, existing over a range of temperature (Gibbs *et al.* 1985), possesses a net moment, and the bunching angle is still rather small. Although the angle  $2\phi$  between two bunched planes is almost constant, the exchange interaction distorts the structure near the spin slips so that the moments are not symmetrically disposed around the easy axis. As the temperature is increased further, the bunching decreases and the concept of spin slips becomes less useful. Thus the configuration of Fig. 2.5(d) can be considered as a distorted three spin-slip structure, but it is simpler to regard it as a commensurate, almost regular helix in which every third plane aligns its moments close to an easy axis in order to reduce the anisotropy energy.

The spin-slip structures of Ho have been subjected to a careful and extensive neutron-diffraction study by Cowley and Bates (1988). They interpreted their results in terms of three parameters:

$b$  - the number of lattice planes between spin slips,

$2\alpha$  - the average angle between the moments in a bunched pair,

$\sigma_G$  - a Gaussian-broadening parameter for  $\alpha$ .

In a perfect, undistorted structure,  $\alpha = \phi$  and  $\sigma_G = 0$ . The parameter  $\sigma_G$  takes into account two effects; the distortions which occur in perfect periodic structures such as that illustrated in Fig. 2.5(b), and possible irregularities in the positions of the spin-slip planes. The former is in principle included in the calculations, whereas the latter is not. From the calculated magnetic structures, such as those illustrated in Fig. 2.5, it is possible to deduce the corresponding neutron-diffraction patterns and hence, by fitting the peak intensities, determine the values for  $\alpha$  and  $\sigma_G$  (Mackintosh and Jensen 1990). The parametrization suggested by Cowley and Bates is in practice rather satisfactory; it allows a fit of all the calculated neutron-diffraction intensities, which vary over about five orders of magnitude, with a relative error of in all cases of less than 20%. Furthermore, the parameter  $\alpha$  is close to the average values of the angle  $\phi$  determined directly from the calculated structures. The measured and calculated values of  $\alpha$  are in good agreement, taking into account the experimental uncertainties, but there are some discrepancies in  $\sigma_G$ . It is noteworthy that the agreement between the predicted and observed neutron-diffraction intensities is very good for the  $b = 11$ , one-spin-slip structure, but that the experimental values of  $\sigma_G$  otherwise

lie consistently above the theoretical. This may indicate that the perfect periodicity of the less stable spin-slip structures is more effectively disturbed by imperfections.

As may be seen from Table 2.1, the easy direction in Er is the  $c$ -axis at high temperature, so the moments order in a longitudinal-wave structure at  $T_N$ . As the temperature is reduced, the structure squares up, as discussed in Section 2.1.4. The basic wave-vector  $\mathbf{Q}$  describing the magnetic ordering increases approximately linearly just below  $T_N$  (Atoji 1974; Habenschuss *et al.* 1974). This is not in accord with the quadratic dependence predicted by (2.1.35*b*) and furthermore, since  $\mathcal{J}'(3\mathbf{Q})$  is probably negative, the predicted change in  $\mathbf{Q}$  also has the opposite sign to that observed. This behaviour can only be accounted for if  $\mathcal{J}(\mathbf{q})$  is temperature dependent, as is indicated even more clearly at lower temperatures, where  $\mathbf{Q}$  starts to decrease quite rapidly. At  $T'_N \simeq 52$  K, a basal-plane component begins to order, through the mechanism described in Section 2.1.5. When the temperature is lowered further,  $\mathbf{Q}$  continues to decrease, exhibiting a number of plateaux, and a rich harmonic structure is observed (Atoji 1974; Habenschuss *et al.* 1974; Gibbs *et al.* 1986). Very detailed neutron-diffraction measurements by Cowley (1991) have revealed a whole sequence of commensurate structures with decreasing temperature, with  $Q = 2/7, 3/11, 7/26, 4/15, 5/19, 6/23,$  and  $1/4$ , in units of  $2\pi/c$ . At 18 K, a first-order transition to a steep cone, with an opening angle of  $30^\circ$  and a wave-vector of  $\sim 5/21$ , is observed.

To explain these results, we may employ a modified version of the model of Jensen (1976*b*), in which crystal fields, isotropic exchange, and dipolar interactions are included. In addition, the anisotropic two-ion coupling, which is required by the observed excitation spectrum and discussed in Section 6.1, is also taken into account. Mean-field calculations then predict that the structure in the intermediate temperature range is an elliptic cycloid, the hodograph of which at 48 K, just below the transition temperature, is shown in Fig. 2.6. As discussed in Section 2.1.5, an additional second-order transition may occur below  $T'_N$ , to a phase with a non-collinear, elliptical ordering of the basal-plane moments. In the presence of random domains, the neutron-diffraction patterns from the two structures are essentially indistinguishable, and if this transition occurs in Er, the fluctuations expected near a second-order transition may also be suppressed, because it is then likely that it coincides with one of the first-order commensurate transitions. The model calculations indicate that the non-collinear component in the basal plane is close to becoming stable when the cycloidal phase is disrupted by the first-order transition to the cone phase. Hence it is most probable that the moments in Er are ordered in a planar elliptic-cycloidal structure in the

whole interval between  $T_C$  and  $T'_N$ , but it is possible that a non-collinear basal-plane component is present in some of the commensurate structures just above  $T_C$ .

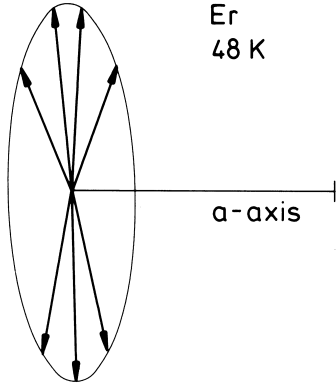


**Fig. 2.6.** The calculated magnetic structure in Er at 48 K. Each arrow represents the magnitude and orientation, in the  $a$ - $c$  plane, of the ordered moment in a specific plane normal to the  $c$ -axis, relative to the magnitude of the moment at absolute zero ( $9\mu_B$ ), indicated by the length of the line along the  $a$ -axis. The hodograph is very close to an ellipse, with semi-axes of length 6.5 and  $2.2\mu_B$ , and this structure can be considered as comprising four planes of moments with a positive component along the  $c$ -axis, followed by three with a negative moment, with the designation (43).

The structure shown in Fig. 2.6 comprises four planes of moments with a positive component along the  $c$ -axis, followed by three with a negative moment. The basic wave-vector is therefore  $2/7$ , and we may describe the structure as (43). The other commensurate structures listed above are then respectively  $2\times(443)$ ,  $2\times(4434443)$ , (4443),  $2\times(44443)$ , (444443), and (44) where, in each case, blocks of  $n$  moments with a positive component along the  $c$ -axis alternate with negative blocks, and the doubling is necessary to ensure periodicity if the number of blocks is odd. These calculations give a good account of the neutron-diffraction results of Cowley (1991). The lattice strains associated with a number of these structures have been studied with synchrotron X-rays by Gibbs *et al.* (1986). The fundamental wave-vector for the oscillating  $c$ -axis strain in a structure like (44), which has inversion symmetry, is twice that of the magnetic structure. However, the other examples above do not have inversion symmetry, so charge-scattering of X-rays may occur at the fundamental magnetic wave-vector. In the cone phase, the X-ray scattering at the fundamental wave-vector of the helical component is anomalously large, even though the longitudinal lattice-strain must be very small. There is however also a contribution from charge scattering associated with a *transverse* strain, discussed at the end of the previous section, which may arise when the mirror symmetry normal to the  $c$ -axis is broken, as it is in this structure. The hexagonal symmetry of a

particular plane is then maintained, but it suffers a lateral displacement which follows the direction of the helical component of the moment.

The transition from the cycloidal to the cone structure in Er at 18 K reflects a shift in the balance between a number of competing effects. At this low temperature, the entropy is not important, since most of the moments are close to their saturation value near  $T_C$ , nor does the difference between the single-ion crystal-field anisotropy energy in the two phases play a significant role. Because of cancellation among the three contributions, the axial anisotropy is relatively insensitive to the angle between the  $c$ -axis and the moments, the average value of which does not, in any case, change much at the transition. The small amplitude of the basal-plane components ensures that the hexagonal-anisotropy energy also has only a minor influence. Hence the choice between the two phases is dominated by the two-ion contributions to the energy. From the spin-wave dispersion relation, discussed in Section 6.1, the difference  $\mathcal{J}_\perp(\mathbf{Q}) - \mathcal{J}_\perp(\mathbf{0})$  is estimated to be about 0.07–0.1 meV, strongly favouring a modulated structure. The tendency towards a modulation of the  $c$ -axis component is opposed by three effects. Firstly, the anisotropy of the classical dipole–dipole contribution reduces  $\mathcal{J}_\parallel(\mathbf{Q}) - \mathcal{J}_\parallel(\mathbf{0})$  by 0.03 meV to about 0.04–0.07 meV. Secondly, the modulated ordering of the  $c$ -axis component cannot take full advantage of the large value of  $\mathcal{J}_\parallel(\mathbf{Q})$ , because of the squaring up which occurs as the temperature is decreased. The energy due to the coupling of the longitudinal component of the moments is

$$U_{\zeta\zeta} = -\frac{1}{4}N \sum_{n \text{ odd}} \mathcal{J}_\parallel(n\mathbf{Q}) \langle J_\zeta(n\mathbf{Q}) \rangle^2 = -\frac{1}{2}N \overline{\mathcal{J}}_\parallel(\mathbf{Q}) \langle |J_\zeta| \rangle^2, \quad (2.3.1a)$$

introducing the effective coupling parameter  $\overline{\mathcal{J}}_\parallel(\mathbf{Q})$ . At high temperatures, close to  $T_N$ , the two coupling parameters  $\overline{\mathcal{J}}_\parallel(\mathbf{Q})$  and  $\mathcal{J}_\parallel(\mathbf{Q})$  are equal, but as the higher odd harmonics gradually develop,  $\overline{\mathcal{J}}_\parallel(\mathbf{Q})$  decreases, and when the structure is close to the square wave, we find from (2.1.36) that

$$\overline{\mathcal{J}}_\parallel(\mathbf{Q}) \simeq \frac{8}{\pi^2} \left\{ \mathcal{J}_\parallel(\mathbf{Q}) + \frac{1}{9} \mathcal{J}_\parallel(3\mathbf{Q}) + \dots \right\}. \quad (2.3.1b)$$

Just above the cone transition, the model calculations indicate that  $\overline{\mathcal{J}}_\parallel(\mathbf{Q})$  is reduced by 0.02–0.03 meV, compared to  $\mathcal{J}_\parallel(\mathbf{Q})$ , which in combination with the dipolar term removes most of the energy difference between the modulated and ferromagnetic ordering of the  $c$ -axis component. The final contribution, which tips the balance into the cone phase below  $T_C$ , is the magnetoelastic energy associated with the  $\alpha$ -strains

$$U_{\text{me}}^\alpha = -\frac{1}{2}(c_{11} - c_{66})(\epsilon_{11} + \epsilon_{22})^2 - \frac{1}{2}c_{33}\epsilon_{33}^2 - c_{13}(\epsilon_{11} + \epsilon_{22})\epsilon_{33}. \quad (2.3.2)$$

The abrupt change in the uniform  $\alpha$ -strains (Rhyne and Legvold 1965b) at the transition to the cone phase reduces this energy by 0.19 meV/ion (Rosen *et al.* 1973), corresponding to an increase of  $\mathcal{J}(\mathbf{0})$  by about 0.01 meV. In the cycloidal phase, there is also a longitudinal-strain mode at wave-vector  $2\mathbf{Q}$ , which disappears in the cone phase, but the energy gained by this distortion is estimated to be very small. Since the  $c$ -axis moment is substantially squared up in the cycloidal phase just above the transition, the change of the  $\alpha$ -strains cannot have its origin in the single-ion magnetoelastic coupling, which does not distinguish between positive and negative moments. It must rather be caused by the strain-dependence of the two-ion interaction

$$\Delta\mathcal{H}_{\text{me}} = - \sum_{ij} [I_1(ij)\{\epsilon_{11}(i) + \epsilon_{22}(i)\} + I_3(ij)\epsilon_{33}(i)] J_{i\zeta} J_{j\zeta}, \quad (2.3.3)$$

which is that part of eqn (2.2.32) which changes at the transition. If the basal-plane moments and the single-ion magnetoelastic terms are assumed to be the same immediately above and below  $T_C$ ,  $\Delta\mathcal{H}_{\text{me}}$  gives rise to the following changes at the transition:

$$\begin{aligned} (c_{11} - c_{66})\Delta(\epsilon_{11} + \epsilon_{22}) + c_{13}\Delta\epsilon_{33} &= N\{I_1(\mathbf{0}) - \bar{I}_1(\mathbf{Q})\}\langle|J_\zeta|\rangle^2 \\ c_{13}\Delta(\epsilon_{11} + \epsilon_{22}) + c_{33}\Delta\epsilon_{33} &= N\{I_3(\mathbf{0}) - \bar{I}_3(\mathbf{Q})\}\langle|J_\zeta|\rangle^2, \end{aligned} \quad (2.3.4)$$

where the bars denote effective coupling parameters, as in (2.3.1), and  $\Delta\epsilon_{\alpha\alpha} = \epsilon_{\alpha\alpha}(\text{cone}) - \epsilon_{\alpha\alpha}(\text{cycloid})$ . Since the elastic constants are known, and the strains are  $\Delta\epsilon_{33} = 3.1 \cdot 10^{-3}$  and  $\Delta(\epsilon_{11} + \epsilon_{22}) = -2.4 \cdot 10^{-3}$ , the two-ion magnetoelastic-coupling parameters may be determined from this equation. The nature of this magnetoelastic contribution implies that it should be possible to suppress the cone phase in Er by applying hydrostatic pressure. In the zero-temperature limit, the energy difference between the two phases is estimated to be only about 0.033 meV/ion, so a hydrostatic pressure of about 2.5 kbar, or alternatively a uniaxial pressure along the  $c$ -axis of only about half this amount, should be sufficient to quench the cone. The application of this modest pressure should then allow experimental studies of the cycloidal phase in Er below 18 K, to ascertain, for example, whether the transition to the phase with an elliptical ordering of the basal-plane moments occurs. We shall return to this two-ion magnetoelastic interaction when we discuss Er films and superlattices.

The negative value of  $B_2^0$  in Tm is large and  $B_6^0$  is also negative, as may be seen in Table 2.1, so that the moments are firmly anchored to the  $c$ -direction, and no ordered basal-plane component appears at any temperature. A longitudinal-wave structure forms at 56 K, and starts to square up at about 40 K, as the amplitude approaches the free-ion

moment of  $7.0\mu_B$ . At 32 K, there is a first-order transition to a commensurate state, with a seven-layer repeat distance, which has a ferromagnetic component (Brun *et al.* 1970). At the lowest temperatures, this has developed into a *ferrimagnetic* square-wave structure, comprising a repeating pattern of four layers of positive moments followed by three of negative moments. These structures, the susceptibility curves of Fig. 2.1, and the excitation spectrum have been used to determine the parameters of a model for Tm with the usual basic ingredients of isotropic exchange, crystal fields, and dipolar interactions (McEwen *et al.* 1991). As shown in Fig. 2.7, the observed squaring-up process is very well accounted for by mean-field calculations based on this model. The principal discrepancy with experiment is in the magnitude of the field along the *c*-axis which is required to form a ferromagnetic structure, where the calculation gives a value about 50% above the observed 28 kOe. This may indicate that the form of  $\mathcal{J}(\mathbf{q})$  in Tm which, as illustrated in Fig. 1.17, has the largest peak in the whole heavy rare earth series, changes substantially at this first-order transition.

The magnetic structures of the light rare earths have not generally been described in the same detail as those of the hcp metals, with the exception of Nd, which has been intensively studied for several decades.

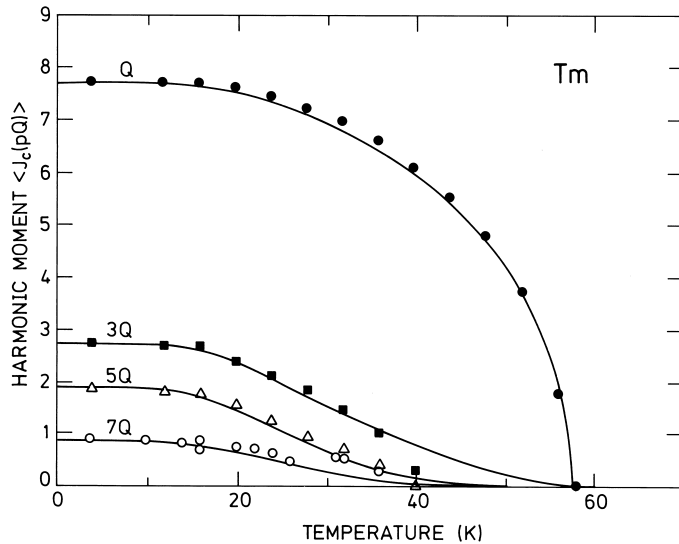


**Fig. 2.7.** The calculated harmonics of the *c*-axis moment in Tm as a function of temperature, compared with the results of neutron diffraction measurements, and the ferromagnetic moment ( $7Q$ ).

Such is the complexity of the observed neutron diffraction patterns, however, that it is only recently that a reasonably complete delineation of the ordered moments has been attained (Zochowski *et al.* 1991). At the Néel temperature of 19.9 K, a weakly first-order transition leads to a longitudinal-wave structure propagating in a  $b$ -direction on the hexagonal sites of the dhcp structure, with an incommensurable periodicity given by  $\mathbf{Q}_h = 0.13\mathbf{b}_1$ . The moments on neighbouring hexagonal layers are ordered antiferromagnetically. Simultaneously, a  $c$ -axis moment (plus a small component in the basal plane) with the same  $\mathbf{Q}$  is induced on the cubic sites by the anisotropic two-ion coupling. The moments on neighbouring cubic layers are also ordered antiferromagnetically. As the temperature is further lowered, another first-order transition at 19.2 K establishes a double- $\mathbf{Q}$  structure, with wave-vectors  $\mathbf{Q}_1$  and  $\mathbf{Q}_2$  aligned approximately along a pair of  $b$ -axes but canted slightly, so that the angle between them is somewhat less than  $120^\circ$ . The polarization vectors of the moments in the two waves are also canted away from the corresponding  $b$ -axes and towards each other, but by a different amount from the wave-vectors, so that the waves are no longer purely longitudinal. Compared with the single- $\mathbf{Q}$  structure, this arrangement increases the average ordered moment, which is further augmented, as the temperature is lowered, by a squaring-up of the structure, which generates harmonics in the neutron-diffraction pattern. Simultaneously, the period gradually increases. At 8.2 K, the planar components of the moments on the cubic sites begin to order, and after undergoing a number of phase transitions, the structure at low temperatures is characterized by the four  $\mathbf{Q}$ -vectors illustrated in Fig. 2.8. Although all four periodicities are present on each type of site,  $\mathbf{Q}_1$  and  $\mathbf{Q}_2$ , which are now aligned precisely along  $b$ -axes, but have different magnitudes  $0.106b_1$  and  $0.116b_1$ , generate the dominant structures on the hexagonal sites, while  $\mathbf{Q}_3$  and  $\mathbf{Q}_4$ , which have lengths  $0.181b_1$  and  $0.184b_1$  and are canted towards each other, predominate on the cubic sites. The different types of  $\mathbf{Q}$ -vector are interrelated; within the experimental uncertainty  $\mathbf{Q}_3 + \mathbf{Q}_4 = 2\mathbf{Q}_1$ , and the canting of  $\mathbf{Q}_3$  and  $\mathbf{Q}_4$  is related to the difference in length between  $\mathbf{Q}_1$  and  $\mathbf{Q}_2$ .

The explanation of these structures from first principles in terms of the elementary magnetic interactions is clearly a formidable task but, as we have seen in Section 2.1.6, the ordering on the hexagonal sites at high temperatures can be satisfactorily accounted for by a phenomenological Landau expansion of the free energy in terms of the order parameters, and the role of the different interactions thereby clarified. The anisotropic two-ion coupling between the dipoles confines the moments to the basal plane and tends to favour the longitudinal-wave structure. Two-ion coupling between the quadrupoles, proba-

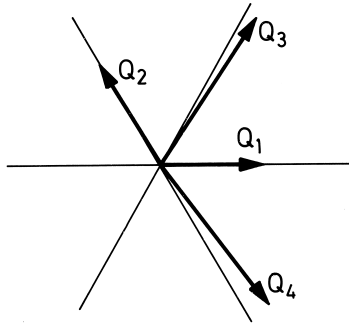


**Fig. 2.8.** The relative orientations and magnitudes of the fundamental wave-vectors which describe the quadruple- $\mathbf{Q}$  magnetic structure of Nd at low temperatures. All four periodicities are present on each type of site, but  $\mathbf{Q}_1$  and  $\mathbf{Q}_2$  generate the dominant structures on the hexagonal sites, while  $\mathbf{Q}_3$  and  $\mathbf{Q}_4$  predominate on the cubic sites.

bly of magnetoelastic origin, lifts the degeneracy between the different multiple- $\mathbf{Q}$  structures and stabilizes the single- $\mathbf{Q}$  state just below  $T_N$ . The Landau expansion can also explain the rotation of the wave-vectors and moments away from the  $b$ -axes, with the consequent stabilization of the double- $\mathbf{Q}$  configuration, and account for the observed harmonics in this structure. A similar analysis for the quadruple- $\mathbf{Q}$  structure in the low-temperature region would provide the basis for understanding the even more complicated phenomena which are observed when a magnetic field is applied to Nd (Zochowski *et al.* 1991).

### 2.3.2 The magnetization of Holmium

The analytical mean-field treatment by Nagamiya *et al.* (1962) of the effect of a magnetic field applied in the plane of a helical structure was mentioned in Section 1.5. As the field is increased, the helix first distorts, giving rise to a moment along  $\mathbf{H}$ , and then undergoes a first-order transition to a fan structure, in which the moments oscillate about the field direction. A further increase in the field reduces the opening angle of the fan which, in the absence of magnetic anisotropy, goes continuously to zero, establishing a ferromagnetic phase at a second-order transition. Hexagonal anisotropy may modify this process by inducing a first-order transition or, if it is large enough, eliminate the fan phase entirely.

The magnetization curves measured by Strandburg *et al.* (1962) and Féron (1969) behaved in accordance with this description at low temperatures, but above about 40 K when the fan phase was first observed, a further phase also appeared, manifested by a plateau corresponding to a moment about one half of that attained in the fan phase. This extra phase was clearly apparent in the magnetoresistance measurements of Mackintosh and Spanel (1964), and later experiments by Akhavan and Blackstead (1976), in which the field was changed continuously, revealed

as many as five different phases at some temperatures. The structures in a magnetic field were investigated with neutron diffraction by Koehler *et al.* (1967), who identified two intermediate phases which they called fans and characterized by the intensity distribution of the Bragg peaks.

These phenomena have been elucidated by means of calculations of the effect of a magnetic field on the commensurate structures of Fig. 2.5 (Jensen and Mackintosh 1990). At low temperatures, the hexagonal anisotropy has a decisive influence on the magnetic structures, ensuring that a first-order transition occurs from the helix or cone to the ferromagnet, without any intermediate phases. Below about 20 K, where the cone is the stable structure in zero field, the cone angle is almost independent of the applied field in the basal plane, but at the transition to the ferromagnet, the  $c$ -axis moment disappears. When the field is applied in the hard direction at these temperatures, the moments just above the ferromagnetic transition do not point along the field direction, but are aligned very closely with the nearest easy axis, so that  $\langle J_{\parallel} \rangle \simeq 8 \cdot \sqrt{3}/2$ , as illustrated in Fig. 1.20. As the field is further increased, they turn towards it, becoming fully aligned through a second-order phase transition at a critical field which is estimated from  $B_6^6$  to be about 460 kOe at absolute zero. At low temperatures, the hexagonal anisotropy also hinders the smooth distortion of the helix in a field. The moments jump discontinuously past the hard directions as the field is increased, giving first-order transitions which may have been observed, for example, as low-field phase boundaries below 20 K in the measurements of Akhavan and Blackstead (1976).

Above about 40 K, when the hexagonal anisotropy is not so dominant, intermediate stable phases appear between the helix and the ferromagnet. The nature of these phases may be appreciated by noting that the helix can be considered as blocks of moments with components alternately parallel and antiparallel to the field, as is apparent from the structures illustrated in Fig. 2.5. If we write this pattern schematically as  $(+ - + -)$ , then the fan structure may be described as  $(+ + + +)$ . The intermediate structures, the helifans, then correspond to patterns of the type specified in Table 2.2. The notation  $\text{helifan}(p)$  is used to designate a structure whose fundamental period is  $p$  times that of the helix (the single number  $p$  is not generally adequate for discriminating between the different helifans). It is clear that these structures represent compromises between the demands of the exchange for a periodic structure, and the field for a complete alignment of the moments. They are not due to the hexagonal anisotropy which, on the contrary, tends to suppress them, and occur both when the field is applied along the easy and hard directions in the plane. The free energies of the various magnetic phases as a function of magnetic field in the easy direction at

**Table 2.2.** The arrangement of blocks of spins in the helifan structures. The first row shows the relative number of  $(-)$  blocks in the different structures.

Helix	Helifan				Fan
	(4)	(3)	(3/2)	(2)	
1/2	3/8	1/3	1/3	1/4	0
+	+	+	+	+	+
-	+	+	+	+	+
+	+	+	-	+	+
-	-	-	+	-	+
+	+	+	+	+	+
-	-	-	-	+	+
+	+	+	+	+	+
-	-	+	+	-	+
+	+	+	-	+	+
-	+	-	+	+	+
+	+	+	+	+	+
-	-	-	-	-	+

50 K are shown in Fig. 2.9. In these calculations, the wave-vector  $\mathbf{Q}$  was allowed to vary in small, discrete steps, by changing the repeat distance, and the absolute minimum in the free energy for the structure thereby determined, as illustrated in the insert to Fig. 2.9, leading to the prediction that the stable magnetic structures follow the sequence helix  $\rightarrow$  helifan(3/2)  $\rightarrow$  fan  $\rightarrow$  ferromagnet as the field is increased. The helifan(3/2) is depicted in Fig. 2.10. In a narrow interval between the helix and the helifan(3/2), other stable phases appear, e.g. the helifan(4') (+ + - + + - + -), and similarly a sequence of helifans with  $m$  (+) blocks followed by a  $(-)$  ( $m \geq 3$ ) occurs in the close neighbourhood of the fan phase. The various structures are associated with characteristic neutron-diffraction patterns. An examination of the neutron-diffraction intensities which Koehler *et al.* (1967) associate with the phase which they designate as 'Fan I' reveals a striking correspondence with the helifan(3/2) pattern, with a very weak fundamental at  $\mathbf{Q}_0/3$ , where  $\mathbf{Q}_0$  is approximately the wave-vector of the helix, strong second and third harmonics, and a weak fourth harmonic. The basic periodicities of this structure are  $2\mathbf{Q}_0/3$  for the component of the moments parallel to the field, and  $\mathbf{Q}_0$  for the perpendicular component; the weak  $\mathbf{Q}_0/3$  peak arises as the result of interference between them. Similar but more detailed neutron-diffraction results have more recently been obtained by Axe *et al.* (1991). The changes in the basic wave-vector are substantial,

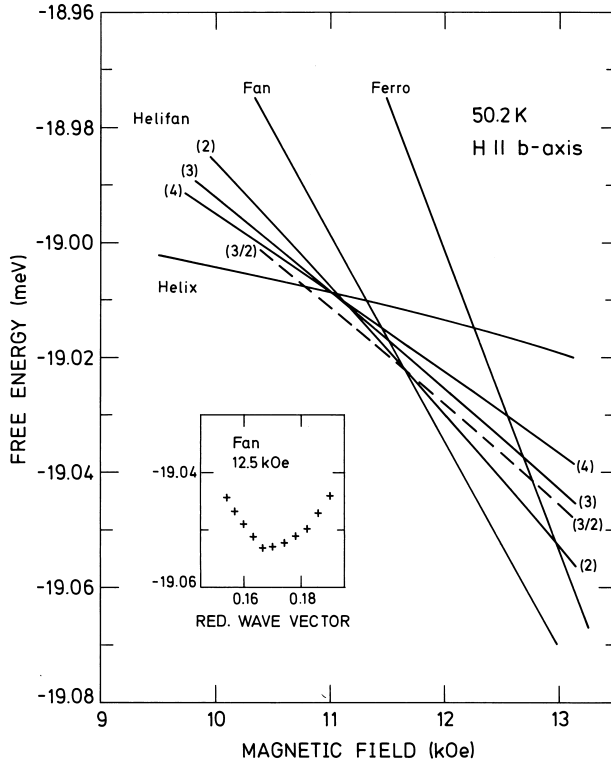


**Fig. 2.9.** Mean-field calculation of the free energy per ion for different magnetic structures in Ho at 50 K, as a function of the magnetic field along an easy  $b$ -axis. The free energy is in each case minimized with respect to the wave-vector which characterizes the structure, as illustrated for the fan phase in the insert.

even though the underlying exchange function is constant, and they agree very well with those observed by neutron diffraction. For the helix, fan and helifan(3/2) structures, the experimental (theoretical) values of  $Q$  are respectively 0.208 (0.211), 0.170 (0.168), and 0.063 (0.066), times  $2\pi/c$ . The period of the fan phase increases relative to that of the helix because of the resulting increase in the opening angle of the fan, expressed by the relation (1.5.21). This allows a decrease in the exchange energy which is greater than the concomitant increase of the Zeeman energy. The change in  $Q$  in the various helifan phases is therefore to a very good approximation proportional to their magnetization.

## Helifan (3/2)

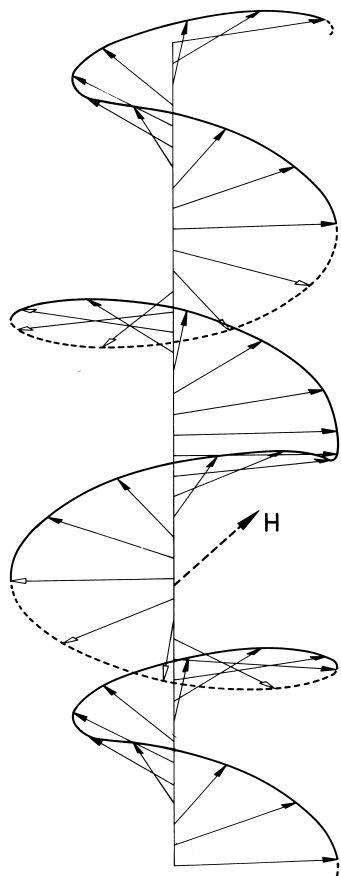


**Fig. 2.10.** The helifan(3/2) structure in Ho at 50 K. The moments lie in planes normal to the  $c$ -axis and their relative orientations are indicated by arrows. A magnetic field of 11 kOe is applied in the basal plane, and moments with components respectively parallel and antiparallel to the field are designated by filled and open arrow-heads. This component of the moments has a periodicity which is 3/2 that of the corresponding helix, and the helicity of the structure changes regularly.

A detailed consideration (Mackintosh and Jensen 1990) of the magnetization curves measured in Ho indicates that the metastable helifan(2) may replace or co-exist with the stable (3/2)-structure, if the measurements are made so rapidly that complete thermodynamic equilibrium is not attained. Other stable or metastable helifans may be involved in the five phases observed by Akhavan and Blackstead (1976). In addition, the very pronounced hysteresis which they observed is consistent with the existence of a large number of phases which have almost the same energy, but are not easily transformed into each other.

The stability of the various periodic structures is determined by the form of the two-ion coupling, especially the long-range component. If

the exchange is sufficiently short-range, the helix, helifans and fan are almost degenerate at the critical field; it is the interaction between the blocks which differentiates between these structures. One of the most remarkable features of the helifans is the large number of hexagonal layers involved in a single period, a characteristic which they share with the commensurable structures observed in zero field in Ho and Er, which were discussed in the preceding sub-section.

Helifans, or analogous structures, may also occur in other rare earth systems where periodic ordering is observed. For example, the modulated structures in Nd discussed previously may be described as  $(+ - + - + - + -)$ , indicating blocks of moments with a component parallel or antiparallel to a magnetic field applied in the basal plane. A periodic reversal of  $(-)$  blocks will then generate subharmonics of the basic  $\mathbf{Q}$ -vector. Thus the sequence  $(+ + + - + - + -)$  generates  $\mathbf{Q}/4$ , and  $(+ + + - + + + -)$  gives  $\mathbf{Q}/2$ , both of which have been observed by neutron diffraction in a magnetic field (Zochowski *et al.* 1991).

### 2.3.3 Films and superlattices

The development of the technique of *molecular-beam epitaxy* has allowed the fabrication on a substrate of films of rare earth metals, with thicknesses ranging from a few to thousands of atomic planes. In addition, *superlattices*, or *multilayers*, of the form  $[A_l B_m]_n$  may be produced, in which blocks comprising  $l$  planes of element A, followed by  $m$  planes of element B, are replicated  $n$  times. It is clear that an endless variety of such systems may be constructed, and the field is in a stage of rapid development. We will restrict ourselves to a discussion of some of the new physical principles involved in understanding the magnetic properties of such structures, illustrated by a few specific examples.

The essential difference between these structures and a bulk crystal lies, of course, in the boundary conditions. Films and superlattices are *finite* in one dimension, whereas a bulk crystal is assumed to be essentially unbounded, and the magnetic layers are terminated by a medium which may have very different magnetic properties, be it a vacuum, a rare earth with quite different moments and interactions, or a nominally non-magnetic metal such as Y, which is a very popular choice for the intermediate layers in superlattices.

The influence of the finite size on the orientation of the ordered moments is illustrated in Fig. 2.11, which depicts the results of a mean-field calculation, based on the model of Larsen *et al.* (1987), for a 15-plane slab of Ho at 4 K. The bunched commensurable helix encompassing the inner 12 planes is enclosed by a single and a double plane, aligned almost ferromagnetically with the respective outer planes. These ferromagnetic clusters distort the adjacent bunched pairs in a manner reminiscent of

spin slips. Such ferromagnetic terminations at the surfaces of slabs containing planes of rotating moments are a general feature, reflecting the predominantly ferromagnetic interaction between closely neighbouring planes in the magnetic rare earths. This coupling normally gives rise to a net moment in the slab, and is calculated to stabilize ferromagnetic ordering at 4 K in samples thinner than about nine atomic planes (Bohr *et al.* 1989).

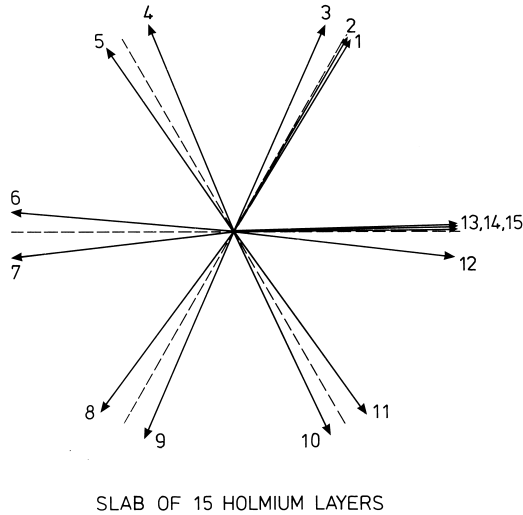


**Fig. 2.11.** Mean-field calculation of the orientation of the magnetic moments in a 15-plane slab of Ho at 4 K. The inner planes are close to a bunched commensurable helix, but there is a strong tendency to ferromagnetism near the surfaces.

The effect of the epitaxial strain is strikingly illustrated by the behaviour of thin films and superlattices of Dy and Er grown on Y, in both of which ferromagnetism is suppressed, by somewhat different mechanisms, in favour of periodic magnetic ordering. In 16-plane Dy films embedded in Y in a variety of  $[\text{Dy}_{16}|\text{Y}_m]$  multilayers, with the  $c$ -axis normal to the plane of the slab, Rhyne *et al.* (1989) found that the helix persists to the lowest temperatures, and the ferromagnetic state is only induced if a field of the order of 10 kOe is applied in the easy direction. An obvious mechanism for this quenching of ferromagnetism is the constraint which the Y slabs impose on the Dy layers, so that the  $\gamma$ -strains which provide the principal driving force for the transition cannot be fully developed.

The ferromagnetic ordering of the axial moment is also suppressed

in  $c$ -axis films and superlattices of Er (Borchers *et al.* 1988), but the explanation in this case is not quite so evident. The dipolar energies are unchanged in the films, nor is it likely that the anisotropy and exchange contributions are decisively different. The strain-dependence of the exchange energy, expressed in eqn (2.3.3), can however provide a mechanism. Y has a planar lattice-constant  $a$  of 3.648 Å, which is over two per cent greater than that of Er, and the Y substrate therefore imposes a strain on the Er film, which is measured to be  $\epsilon_{11} = \epsilon_{22} \simeq 6 \times 10^{-3}$ . If the atomic volume is assumed to be unchanged in the film,  $\epsilon_{33} \simeq -12 \times 10^{-3}$ . The difference in exchange energy between the solid and a thin film may then be found from (2.3.4), and is equivalent to a field of 13 kOe acting on the  $c$ -axis moment of about  $8 \mu_B$ . The above estimate of  $\epsilon_{33}$  is probably too great, so this calculation may be considered in reasonably good agreement with the observation that Er films with thicknesses between 860 Å and 9500 Å require fields varying linearly between 8 kOe and 3 kOe to establish a ferromagnetic state at 10 K. It is noteworthy that, since Lu has a significantly smaller basal-plane lattice-constant than Er, the cone structure should be favoured in a  $c$ -axis epitaxial film grown on Lu.

Many of the characteristic features of rare earth superlattices are demonstrated by the aforementioned [Dy|Y] systems, which are observed to form helical structures over the whole temperature range of magnetic ordering. When the  $c$ -axis is normal to the plane of the film, a coherent magnetic structure may be formed, in which the phase and chirality of the helix are maintained over many bilayers, provided that the slabs of non-magnetic Y are not too thick. The coherence length may be estimated from the widths of the neutron-diffraction peaks, and corresponds to more than 10 bilayers if the Y layers are less than about 10 planes thick. If the thickness is increased to about 35 planes, however, the coherence length, which is inversely proportional to the width of the Y layers, is less than the bilayer thickness, so that the helix in one Dy layer is uncorrelated with that in the next. In the long-range coherent structures, the phase change of the helix across the Dy layers corresponds to a turn angle which varies with temperature and shows a tendency to lock in to  $30^\circ$ , with associated bunching. The phase change across the Y layers, on the other hand, is independent of temperature and the turn angle takes the much larger value of about  $50^\circ$ , which is characteristic of the periodic structures formed by dilute alloys of magnetic rare earths in bulk Y. It therefore appears that the magnetic order is propagated through the Y layers by a spin-density wave, which is incipient in the unperturbed metal, and is associated with the very large susceptibility  $\chi(\mathbf{Q})$  of the conduction electrons. The helical ordering in the Dy layers of the  $c$ -axis superlattice is disturbed by edge effects of the type illustrated for the Ho film in Fig. 2.11. Consequently, the ordered helical

moment falls below the saturation value of  $10\mu_B$  at low temperatures, even though the total integrated magnetic scattering corresponds to the fully saturated moment. At higher temperatures, the coupling of the net ferromagnetic moment in a Dy layer to an applied magnetic field breaks the coherence of the helical structure between the layers well before the transition to the true ferromagnetic phase occurs. A  $b$ -axis superlattice, on the other hand, fails to form a coherent magnetic structure even when the Y layer is as thin as 9 planes, since the static susceptibility at  $\mathbf{q} = \mathbf{0}$ , which is required to propagate the ferromagnetic coupling between the basal planes of the Dy layers through the Y, is not particularly high. The Dy layers therefore form helical magnetic structures with wave-vectors in the plane of the layers, but no coherence of phase or chirality between the layers.